

## Article

# Effect of Doping Trace Rare Earth Elements on Corrosion Behavior of EH36 Offshore Platform Steel

Shujia Zheng<sup>1</sup>, Na Liu<sup>1</sup>, Yang Liu<sup>1</sup>, Xiaoning Wang<sup>2,\*</sup>, Lina Qiu<sup>1,3,\*</sup> and Aijun Gong<sup>1,3</sup> 

<sup>1</sup> College of Chemistry and Biological Engineering, University of Science and Technology Beijing, Beijing 100083, China

<sup>2</sup> Student Affairs Department, University of Science and Technology Beijing, Beijing 100083, China

<sup>3</sup> Beijing Key Laboratory for Science and Application of Functional Molecular and Crystalline Materials, University of Science and Technology Beijing, Beijing 100083, China

\* Correspondence: wxn@admin.ustb.edu.cn (X.W.); qiulina@ustb.edu.cn (L.Q.)

**Abstract:** EH36 offshore platform steel, La (0.0031%) steel, Ce (0.0027%) steel, and Pr (0.0001%) steel were selected as the research objects. The corrosion of four groups of steel was simulated by immersion experiments. In the presence of Cl<sup>-</sup> the effect of rare earth elements (La, Ce, Pr) on corrosion was investigated by the weight loss method. The morphology of the corrosion products and the apparent morphology after the removal of the corrosion products were observed by scanning electron microscopy (SEM); the main components of four steel corrosion products were analyzed by X-ray diffraction (XRD). The electrochemical behavior and the influence of temperature and Cl<sup>-</sup> concentration on the corrosion of the four kinds of steel were analyzed by an electrochemical polarization curve and Nyquist diagram. The results showed that the addition of trace rare earth elements, La, Ce, and Pr, to EH36 offshore platform steel can reduce the corrosion rate and the corrosion current density (*I*<sub>corr</sub>), and increase the charge transfer resistance during the corrosion process. The *I*<sub>corr</sub> of La steel, Ce steel, and Pr steel is  $6.59 \times 10^{-5} \text{ A}\cdot\text{cm}^{-2}$ ,  $7.57 \times 10^{-5} \text{ A}\cdot\text{cm}^{-2}$ , and  $9.53 \times 10^{-5} \text{ A}\cdot\text{cm}^{-2}$ , respectively, which is lower than that of EH36 steel (*I*<sub>corr</sub> =  $1.82 \times 10^{-4} \text{ A}\cdot\text{cm}^{-2}$ ). The influence of Cl<sup>-</sup> concentration and temperature on the four steels showed the same trend; that is, with the increase in Cl<sup>-</sup> concentration, the corrosion rate first rises and then slows down, and with the increase in temperature, the corrosion rate gradually accelerates. Rare earth elements promote the production of more α-FeOOH in the rust layer, and the compactness of this product plays a certain role in protecting the steel matrix. The addition of trace rare earth elements, La, Ce, and Pr (less than 0.004%), improves the corrosion resistance of EH36 steel.

**Keywords:** EH36 offshore platform steel; rare earth elements; anti-corrosion; electrochemistry



**Citation:** Zheng, S.; Liu, N.; Liu, Y.; Wang, X.; Qiu, L.; Gong, A. Effect of Doping Trace Rare Earth Elements on Corrosion Behavior of EH36 Offshore Platform Steel. *Coatings* **2024**, *14*, 413. <https://doi.org/10.3390/coatings14040413>

Academic Editor: Paolo Castaldo

Received: 28 February 2024

Revised: 27 March 2024

Accepted: 28 March 2024

Published: 30 March 2024



**Copyright:** © 2024 by the authors. Licensee MDPI, Basel, Switzerland. This article is an open access article distributed under the terms and conditions of the Creative Commons Attribution (CC BY) license (<https://creativecommons.org/licenses/by/4.0/>).

## 1. Introduction

EH36 steel is a kind of high-strength ship plate steel, which is widely used in large offshore platforms and key parts of the hull. The marine environment is extremely complex, and EH36 offshore platform steel is often affected by salt concentration, dissolved oxygen, temperature, pH, and so on. The study shows that chloride ions are the core factor affecting corrosion. The corrosion of Cl<sup>-</sup> on metal materials is reflected in two aspects: on the one hand, Cl<sup>-</sup> can destroy the passivated film of metal and cause the material to produce pit corrosion; on the other hand, Cl<sup>-</sup> directly participates in the anodic dissolution process of metal materials [1–3]. When the temperature rises within a certain range, the reaction speed of the cathode and anode process will be accelerated. The corrosion process will be promoted by increasing the temperature of the seawater and accelerating the diffusion rate of dissolved oxygen.

In order to improve the safety and service life of steel, many large steel manufacturing industries pay attention to improving the corrosion resistance of steel. According to statistics, effective protective measures can reduce corrosion loss by 25%~40%. There are

many ways to mitigate corrosion, such as coatings, corrosion inhibitors, and micro-alloying technology [4–7]. Coating anticorrosion is to form a layer of shielding coating on the surface of the metal to isolate the metal from the external environment such as oxygen, water, and corrosion ions, but coating anticorrosion has certain limitations. A corrosion inhibitor generally refers to that it exists in the corrosive medium with a certain concentration, mainly changing the nature of the medium, so that the corrosion of metal materials is reduced. Both coatings and corrosion inhibitors can be used to repress the corrosion of metals under certain conditions, but neither can fundamentally change the corrosion resistance of the metal itself. Alloying refers to the addition of other elements in the refining process to improve the properties of metals. For example, the addition of Mo and V can improve resistance to hydrogen corrosion [8]; the addition of Zr improves the corrosion resistance of as-cast Ti-Al-Nb-Zr-Mo alloy [9]. However, the expensive price of these elements and shrinking mineral resources are not conducive to long-term development.

So many researchers are therefore looking for alternatives to traditional alloyed elements, such as rare earth elements, which have been applied to steel for more than seventy years. The peripheral electron configuration of rare earth elements is  $[Xe]4f^n6s^2$  and  $[Xe]4f^{n-1}5d^16s^2$ , and it is easy to lose outer electrons. Rare earth elements have strong bonding ability with O and S. The elements magnesium, aluminum, and calcium are also commonly used in the iron and steel industry as a deoxidizing desulfurizer, but when added to liquid steel, calcium, and magnesium, they are volatile because of the low boiling point and the high vapor pressure. As early as the 1950s, the United States Carpenter Company tried to add rare earth elements La-Ce in the Cr-Ni system of stainless steel [10], and not only was the solidification organization refined, but the steel hot workability was also improved. With the continuous research on rare earth steels, the role of rare earth elements in purifying the steel, modifying modified inclusions, and improving the strength and corrosion resistance of steels is gradually being discovered [11]. There are two main ways in which rare earth elements can improve the corrosion resistance of steel, either by changing the composition and size of inclusions, or by promoting the production of more stable and dense rust layers. MnS and  $Al_2O_3$  are undesirable inclusions commonly found in EH36 offshore platform steel. Li [12] added different contents of Ce to EH36 steel, and MnS was metamorphosed into a spherical composite  $Ce_2O_2S$ -MnS inclusions with one-fifth of the original size. The irregularly shaped  $Al_2O_3$  also changed to spherical composite inclusions with a size of 1.5  $\mu m$  instead of 5  $\mu m$ . Huang et al. [13] investigated the effect of La-Ce on HRB400E steel inclusions as well as corrosion resistance properties. It was found that MnS changed into composite rare earth inclusions and the corrosion rate was reduced by 1.499 mm/a. The rare earth elements promote the production of  $\alpha$ -FeOOH, which is a stable corrosion product with a protective effect on the steel substrate. Dong et al. [14,15] verified the effect of Ce on offshore platform steels and they found that the steel containing Ce had better corrosion resistance properties, a more compact rust layer, and higher  $\alpha$ -FeOOH content.

In many current studies, the rare earth content of steels usually ranges from 0.004% to 0.02% [16–19]. However, more rare earth content will form large particles of rare earth inclusions [20]. This will not only clog the casting nozzles during continuous casting and affect productivity, but also reduce the corrosion resistance. Xi [21] produced steels with a Ce content of 0.006%, 0.012%, and 0.018%, respectively. The corrosion resistance increased and then decreased with increasing rare earth content, while the size of inclusions was smallest for Ce content of 0.012%. Adding ultra-trace rare earth into steel can effectively avoid the “nodule” phenomenon [15], and improve the production efficiency of offshore platform steel. The price of La, Ce, and Pr is moderate, and the content is higher than that of other rare earth elements. In this paper, La (0.0031%), Ce (0.0027%), and Pr (0.0001%) rare earth steels were used as experimental materials, and studied by means of weekly immersion corrosion, electrochemical corrosion, XRD, and SEM with the aim of investigating the effect of ultra-trace rare earth elements (less than 0.004%) on EH36 steel. This will provide

a certain reference for the full utilization of rare earth resources and the development of new rare earth marine platform steel.

## 2. Materials and Methods

### 2.1. Material and Specimen Preparation

In this test, the EH36 offshore platform steel was produced by a steel mill that conforms to the international standard. The EH36 offshore platform steel was marked as 0#, and its main components are shown in Table 1. Three kinds of rare earth steel were prepared by adding La, Ce, and Pr elements to EH36 offshore platform steel in a certain proportion. The vacuum induction melting furnace was evacuated to 20 Pa and charged with argon at room temperature. EH36 offshore platform steel was heated until molten and rare earth elements were added by insertion method. After casting ingot, rolling, multiple rolling, and normalizing treatment, three kinds of rare earth offshore platform steel doped with La, Ce, and Pr, respectively, were obtained. The content of rare earth elements was analyzed by ICP-MS, and the results are shown in Table 2.

**Table 1.** Main chemical composition of 0# (EH36 steel) (wt%).

Sample	Fe	C	Si	Mn	P	S	RE
0# (EH36)	Bal.	0.1118	0.1994	1.5595	0.0156	0.0039	0

**Table 2.** Rare earth element content of rare earth steel (wt%).

1# (La Steel)	2# (Ce Steel)	3# (Pr Steel)
0.0031	0.0024	0.0001

### 2.2. Determination of Corrosion Rate of EH36, La, Ce, and Pr Steel

The steel plate was cut into a sample with a size of 30 mm × 10 mm × 3 mm, and a hole with a diameter of 2 mm was made in the middle of the upper part of the sample for corrosion weightlessness experiments. The surface of the sample was polished with 400, 800, 1200, and 2000 mesh sandpaper on the grinding machine until the surface was bright and without obvious scratches. The polished samples were cleaned separately with absolute ethanol, and dried in the air. The weight before corrosion was recorded as  $M_1$ , and the size of the steel sheet was measured with a vernier caliper. The steel sheets were immersed in 3.5 wt% NaCl solution at 25 °C for 7 d, 14 d, 21 d, 35 d, and 63 d, and each experiment was conducted in parallel three times. After corrosion, the sample was immersed in a solution of 500 mL concentrated hydrochloric acid ( $\rho = 1.19 \text{ g}\cdot\text{mL}^{-1}$ ), 500 mL deionized water, and 3.5 g hexamethyltetramine to remove the stubborn corrosion products. The samples after rust removal were cleaned with deionized water and absolute ethanol, and the weight was recorded as  $M_2$ . The corrosion rates of the four types of steel were calculated according to Equation (1).

$$V_t = 8.76 \times 10^7 \times (M_1 - M_2) / STD \quad (1)$$

$V_t$  is the corrosion rate, mm/a;  $M_1$  and  $M_2$  are the weight before and after corrosion, respectively, g;  $S$  is the total surface area of the sample,  $\text{cm}^2$ ;  $T$  is the soaking time, h;  $D$  is the density of the material,  $\text{kg}/\text{m}^3$ .

### 2.3. Characterization of Corrosion

The macroscopic morphology after corrosion was recorded by camera. SEM (ZEISS GeminiSEM 500, ZEISS, Jena, Germany) was used to observe the microscopic morphology of the products after 63 d corrosion and the surface of the steel after 7 d corrosion.

The surface rust layer was gently scraped with the blade for XRD (Rigaku Ultima IV, Rigaku, Tokyo, Japan) test. By means of a continuous scanning method on a copper target,

with a scanning range from 10 to 80 degrees. The test voltage and current are 40 kV and 40 mA, respectively.

#### 2.4. Electrochemical Measurements

Samples with dimensions of 10 mm × 10 mm × 2 mm were used for electrochemical experiments. One side of the sample was welded with copper wire and sealed with epoxy resin (the weight ratio of epoxy resin to curing agent is 10:0.9). The exposed surface of the sample was polished with 400 mesh, 800 mesh, 1200 mesh, and 2000 mesh sandpaper in turn, and then polished with w2.5 and w0.5 polishing paste on polishing cloth until the sample surface achieved mirror effect. The electrochemical test experiments were carried out in CHI760e electrochemical workstation. All electrochemical experiments used a three-electrode system, which was composed of saturated calomel electrode as reference electrode (RE), platinum sheet electrode as auxiliary electrode, and the sample with different corrosion periods as working electrode (WE). The test electrolytes were NaCl solution. The electrochemical test can be started when the open-circuit potential fluctuates below 2 mV in two minutes. Electrochemical impedance spectrographs (EIS) were performed at a frequency range of  $10^{-2}$  to  $10^5$  Hz with a sinusoidal voltage of 10 mV amplitude as the interference signal. The polarization curve tests were carried out at a scan rate of 2 mV/s and the voltage range was  $\pm 5$  mV according to the open circuit potential.

In addition, the Nyquist diagram and polarization curve spectrum of corrosion were tested at 5 °C, 15 °C, 25 °C, 35 °C, and 45 °C to explore the influence of temperature on the corrosion of the steel. The temperature was controlled at 25 °C, and the concentration of  $\text{Cl}^-$  electrolyte was 0.5 wt%, 2 wt%, 3.5 wt%, 5 wt%, and 6.5 wt%, respectively. Nyquist diagram and Tafel polarization curve were used to explore the influence of  $\text{Cl}^-$  concentration on the corrosion.

### 3. Results and Discussion

#### 3.1. Corrosion Weightlessness Experiment

The samples were corroded at  $\text{Cl}^-$  concentration of 3.5 wt%, temperature of 25 °C, and the results of the corrosion rate after 7 d, 14 d, 21 d, 35 d, and 63 d were shown in Table 3. It can be seen from the data in the table that the 7-day corrosion rates of 1# (La), 2# (Ce), and 3# (Pr) samples are 0.1314 mm/a, 0.1352 mm/a, and 0.1401 mm/a, respectively, while the rate of EH36 steel is 0.1509 mm/a. In the initial stage of corrosion, the reason for the low corrosion rate of rare earth steel may be that rare earth elements change the composition and size of inclusions in EH36 offshore platform steel. The larger the inclusion size is, the more corrosion sites there are. Zhang et al. [22–24] found that inclusions tend to form microcracks between steel substrates, and corrosion ions preferentially erode microcracks. Zhang et al. [25] also have similar findings. However, with the extension of time, the four steels show the same corrosion law; that is, the larger the corrosion period, the smaller the corrosion rate. The corrosion rates of the four kinds of steel were reduced to 0.0891 mm/a, 0.0632 mm/a, 0.0804 mm/a, and 0.0825 mm/a, respectively. This may be due to the accumulation of corrosion products on the surface of the steel matrix, forming a protective effect on the steel matrix and hindering the further erosion of  $\text{Cl}^-$ .

**Table 3.** Corrosion rates of four steels after different corrosion cycles (mm/a).

Time (d)	0#	1#	2#	3#
7	0.1509	0.1314	0.1352	0.1401
14	0.1465	0.1278	0.1342	0.1336
21	0.1371	0.1256	0.1320	0.1262
28	0.1300	0.1234	0.1220	0.1239
35	0.1226	0.1138	0.1177	0.1189
63	0.0891	0.0632	0.0804	0.0825

The samples were removed from the corrosion solution, and the macro morphology of the four types of steel after 63 d was recorded, as shown in Figure 1. It can be clearly seen from Figure 1 that some corrosion products on the surface of the 0# sample are relatively light brown-red, and a few are brown-black. Loose corrosion products provide a transport channel for water, oxygen, and corrosive ions, so 0# sample corrosion is more likely to occur, and the corrosion rate will be faster. However, the corrosion products on the surface of 1#, 2#, and 3# samples are dark brown or black, and they are closely covered on the surface of the steel matrix, forming a certain protective effect on the steel matrix, whereby the corrosion is slow. The main components of the brownish-red rust layer are ferrous hydroxide, ferrous oxide, and hydroxy iron oxide, which are converted from free iron ions at the beginning of corrosion. The dark brown and black rust layers are stable corrosion products such as iron oxide and  $\alpha$ -FeOOH [26].



**Figure 1.** Macro morphology of 0#EH36 offshore platform steel, 1#La steel, 2#Ce steel, and 3#Pr steel after 63 d corrosion.

### 3.2. Surface Characterization

In order to further study the influence of lanthanum, cerium, and praseodymium on the corrosion resistance of EH36 offshore platform steel, SEM was used to observe the micro morphology of the surface and products of the four kinds of steel, as shown in Figure 2. Figure 2a<sub>0</sub>–a<sub>3</sub> show the micro morphology of rust removal of 0#, 1#, 2#, and 3# steel with a corrosion cycle of 7 d, respectively. It can be clearly seen that there are obvious corrosion pits on the surface of 0#EH36 steel, which is because the corrosion preferentially occurs around the inclusions at the initial stage of the reaction, and the corrosion continues to expand outward as the inclusions fall off. However, the surfaces of 1#, 2#, and 3# steels, which were doped with rare earth, are flat. This is consistent with the previous results of the corrosion weightlessness experiment. After 63 days of corrosion, there was a large number of accumulated corrosion products on the surface of the sample, as shown in Figure 2b<sub>0</sub>–b<sub>3</sub>. The rust layer covering the surface of the EH36 offshore platform steel matrix is cracked, as can be seen in Figure 2b<sub>0</sub>, which provides a corrosion path for aggressive ions. However, it can be seen from Figure 2b<sub>1</sub>–b<sub>3</sub> that the cracks in the rust layer of rare earth steel are relatively narrow. The corrosion products can adhere to the steel matrix and form a certain protective effect on the rare earth steel surface, which can effectively prevent Cl<sup>−</sup> from eroding steel. The corrosion product diagrams were enlarged, as in Figure 2c<sub>0</sub>–c<sub>3</sub>. Figure 2c<sub>0</sub> shows the corrosion products of EH36 offshore platform steel were loose and wrinkled, with poor compactness and obvious voidness. This wrinkled product is  $\gamma$ -FeOOH [27]. As shown in Figure 2c<sub>1</sub>–c<sub>3</sub>, there were small and obviously spherical corrosion products, which were  $\alpha$ -FeOOH. The corrosion products were densely packed and covered the surface of the steel, forming a certain protective effect on the steel. Therefore, the addition of rare earth can change the type of corrosion products, form more closely covered corrosion products on the surface of steel, and improve the corrosion resistance of steel.

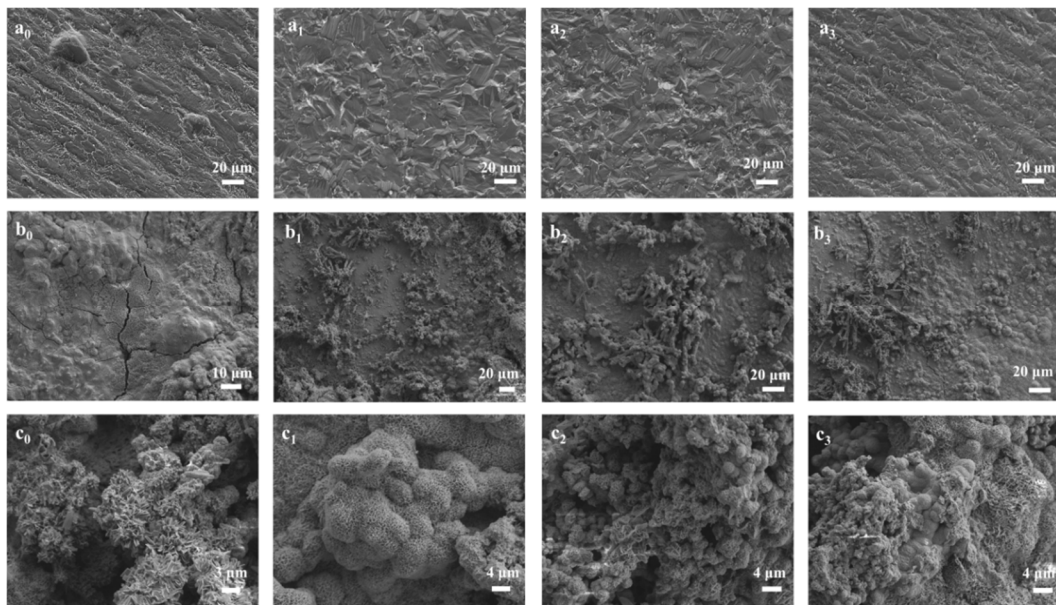


**Figure 2.** SEM diagrams of the rust removal surface after 7 d corrosion of EH36 offshore platform steel ( $a_0$ ) and La steel ( $a_1$ ) and Ce steel ( $a_2$ ) and Pr steel ( $a_3$ ); and the micro morphology diagram of corrosion products after 63 d corrosion of EH36 offshore platform steel ( $b_0$ ) and La steel ( $b_1$ ) and Ce steel ( $b_2$ ) and Pr steel ( $b_3$ ); the corrosion products after 63 d corrosion magnified 2000 times of EH36 offshore platform steel ( $c_0$ ) and La steel ( $c_1$ ) and Ce steel ( $c_2$ ) and Pr steel ( $c_3$ ).

### 3.3. Analysis of Composition of Corrosion Products

To further determine the effect of rare earth elements on the corrosion products, the rust layer after 63 d corrosion was scraped off with a knife, and the main components of the corrosion products were determined by XRD technology. The test results are shown in Figure 3. The corrosion products of the four kinds of steel are mainly composed of  $\alpha$ -FeOOH,  $\gamma$ -FeOOH, and  $Fe_3O_4$ . The corrosion potential of  $\gamma$ -FeOOH is close to that of Fe, and it has electrochemical activity and can be used as a cathode to participate in the reduction reaction.  $\gamma$ -FeOOH is electrochemically active, and the corrosion potential is close to that of Fe, so it can participate in the reduction reaction as a cathode. It can be clearly seen from Figure 3 that after the addition of rare earth elements, the proportion of  $\gamma$ -FeOOH decreased, while the proportion of  $\alpha$ -FeOOH and  $Fe_3O_4$  increased. Studies showed that  $\gamma$ -FeOOH has poor stability and certain electrochemical activity, which is preferentially generated at the initial stage of corrosion and can be gradually transformed into  $\alpha$ -FeOOH and  $Fe_3O_4$ . This transformation process promotes the occurrence of corrosion [28].  $\alpha$ -FeOOH and  $Fe_3O_4$  have insulation, a regular shape, and more stable chemical properties, so they have a protective effect on the matrix and are conducive to improving the corrosion resistance of steel [29]. Some researchers have proposed that the protective parameter of the rust layer ( $\alpha/\gamma$ ) is the mass ratio of  $\alpha$ -FeOOH to  $\gamma$ -FeOOH, and the larger the  $\alpha/\gamma$  value, the stronger the protective effect of the rust layer [30]. Lian et al. [19] studied the influence of mixed rare earth La and Ce on the corrosion of Q235B and Q355B steel, and also found that the rust layer became dense and difficult to fall off after the addition of rare earth La and Ce. The quantitative results of corrosion products showed that the amount of  $\gamma$ -FeOOH decreased while the amount of  $\alpha$ -FeOOH increased in La steel and Ce steel. Combined with the above SEM analysis, it can be seen that doping La, Ce, and Pr can promote the formation of a more stable and dense rust layer  $\alpha$ -FeOOH, which can closely cover the performance of the steel matrix and hinder the transfer of charge and the erosion of corrosive ions. Therefore, the addition of rare earth can improve the corrosion resistance of EH36 offshore platform steel.

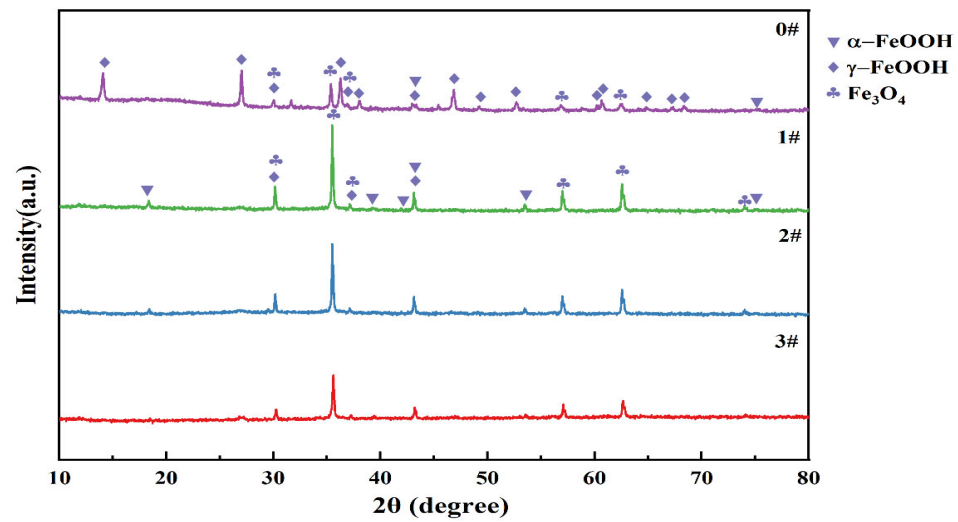


**Figure 3.** XRD patterns of corrosion products of the steel: 0# is EH36 offshore platform steel, 1# is La steel, 2# is Ce steel, and 3# is Pr steel.

### 3.4. Electrochemical Experiments Results

In order to explore the influence of La, Ce, and Pr rare earth elements on the electrochemical corrosion behavior of EH36 offshore platform steel, the impedance spectra of 7 d and 63 d after corrosion and the Tafel polarization curve of 63 d corrosion were measured at the open circuit potential. The impedance test results are shown in Figure 4a,b.

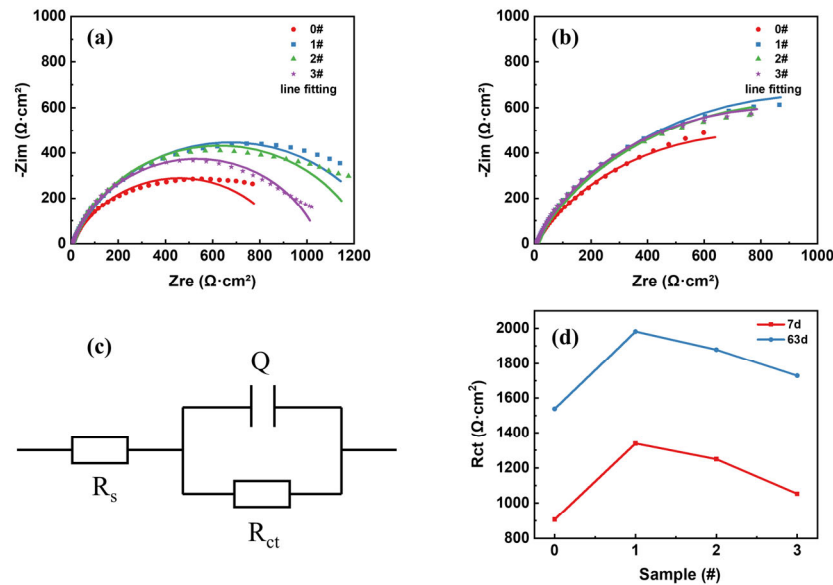


**Figure 4.** Nyquist plots and Rct values (d) of the four steels of 7 d (a); and 63 d (b) corrosion; the Electrochemical equivalent circuit (c).

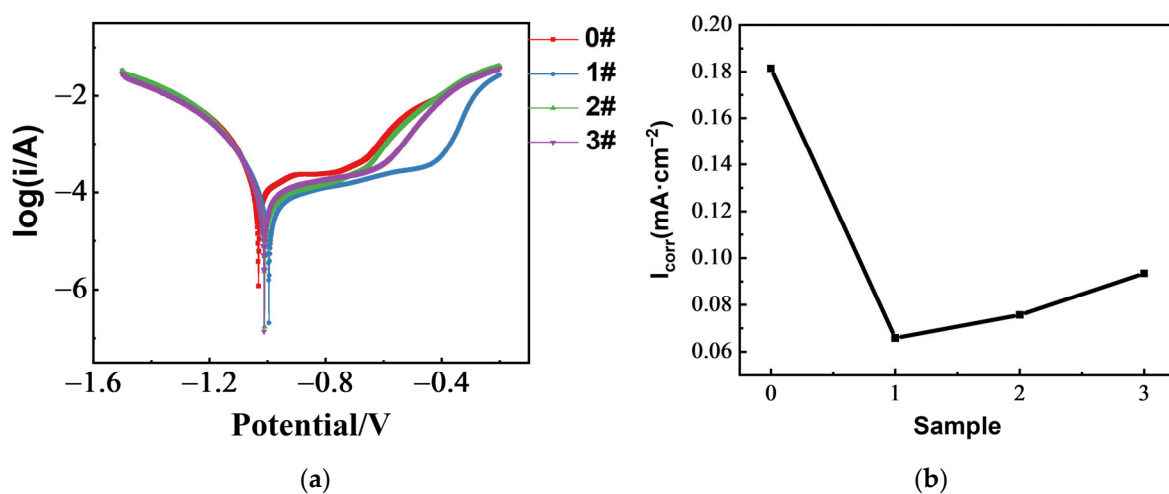
The Nyquist plots of the four kinds of steel in the corrosion solution were composed of one capacitive arc, indicating that the corrosion mechanism of the four kinds of steel was basically the same. The arc radius of the EH36 offshore platform steel was smaller than that of the rare earth steel with La, Ce, and Pr, respectively, indicating that the addition of rare earth improved the corrosion resistance of the steel. The surface of the steel became rough after corrosion, resulting in a non-uniform distribution of the electric field in the electrode–solution interface, which led to a certain difference between the capacitive arc and the fitted ideal arc in the high-frequency region [30]. The Nyquist plots were fitted according to the equivalent circuit shown in Figure 4c to obtain the size of charge

transfer resistance ( $R_{ct}$ ), and the fitting results are shown in Table 4. The comparison of the  $R_{ct}$  value of the four types of steel is shown in Figure 4d. The larger the  $R_{ct}$ , the more corrosion is impeded. By comparing the value of  $R_{ct}$ , it can be seen that the  $R_{ct}$  value after 63 d corrosion was greater than the corresponding value at 7 d, which indicates that the corrosion was less likely to occur with the extension of time. This was due to the protective rust layer of the steel matrix that hindered the erosion of corrosive ions, which was consistent with the previous test results. After 63 d corrosion, the  $R_{ct}$  value of 1#La steel was the largest, which was  $1.98 \times 10^3 \Omega \cdot \text{cm}^2$ , followed by 2#Ce steel ( $1.88 \times 10^3 \Omega \cdot \text{cm}^2$ ) and 3#Pr steel ( $1.73 \times 10^3 \Omega \cdot \text{cm}^2$ ). These three values were greater than the  $R_{ct}$  of EH36 steel ( $1.54 \times 10^3 \Omega \cdot \text{cm}^2$ ), which indicates that the rare earth elements La, Ce, and Pr can improve the density of rust layer, hinder the infiltration of  $\text{Cl}^-$ , and improve the corrosion resistance of EH36 sheet steel during long-term corrosion.

**Table 4.** Fitted values of  $R_{ct}$  ( $\Omega \cdot \text{cm}^2$ ) after 7 d and 63 d corrosion of 0# (EH36 steel), 1# (La steel), 2# (Ce steel), and 3# (Pr steel).

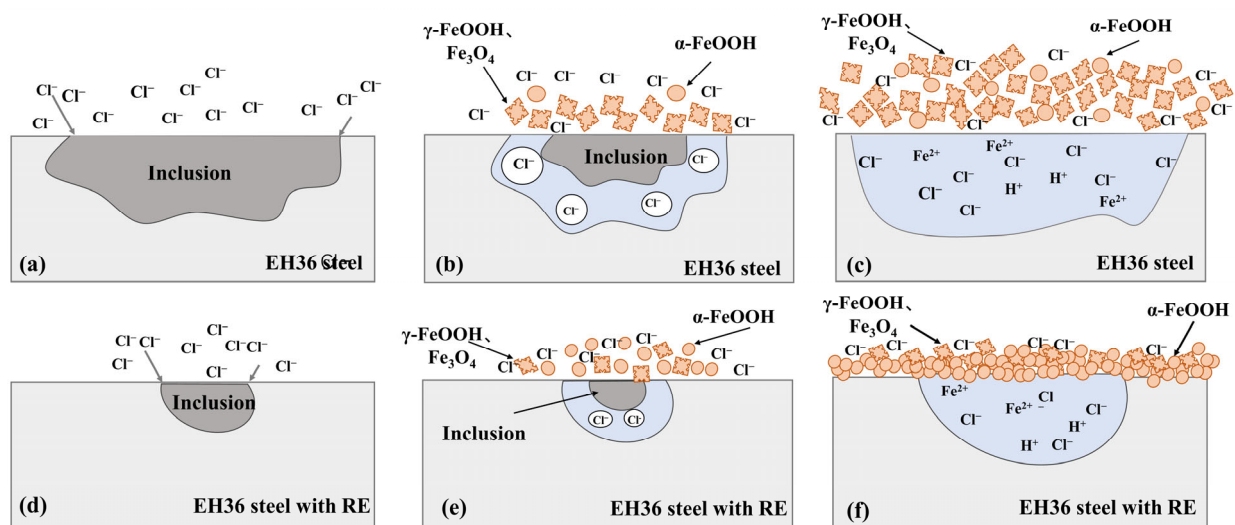
Sample	7 d	63 d
0#	$9.06 \times 10^2$	$1.54 \times 10^3$
1#	$1.34 \times 10^3$	$1.98 \times 10^3$
2#	$1.25 \times 10^3$	$1.88 \times 10^3$
3#	$1.05 \times 10^3$	$1.73 \times 10^3$

Figure 5a shows the Tafel polarization curves after 63 d corrosion. The cathode polarization curve represented the process of oxygen diffusion while the anode represented the process of steel dissolution. The polarization curves of the four steels were very similar, and the cathodic polarization curves almost coincide. With the increase in anode potential, the anode current increased continuously, the anodization curve of La, Ce, and Pr steel shifted to the lower right, and the dissolution speed slowed down. The corrosion current density ( $I_{corr}$ ) is positively correlated with the corrosion rate; that is, the smaller the corrosion current density, the smaller the corrosion rate. The  $I_{corr}$  of 0#EH36 offshore platform steel, 1#La steel, 2#Ce steel, and 3#Pr steel was  $1.82 \times 10^{-4} \text{ A} \cdot \text{cm}^{-2}$ ,  $6.59 \times 10^{-5} \text{ A} \cdot \text{cm}^{-2}$ ,  $7.57 \times 10^{-5} \text{ A} \cdot \text{cm}^{-2}$ , and  $9.53 \times 10^{-5} \text{ A} \cdot \text{cm}^{-2}$ , respectively. It was obvious that the  $I_{corr}$  of EH36 steel was greater than that of the latter three rare earth steels. This was consistent with the results of corrosion weight loss, which further proves that doping rare earth elements La, Ce, and Pr reduced the corrosion rate and improved the corrosion resistance of EH36 offshore platform steel.



**Figure 5.** Tafel curves (a) and the  $I_{corr}$  (b) of the four steels after 63 d corrosion.

Figure 6 shows the corrosion process of EH36 with and without rare earth elements: (a) and (d) is the initial corrosion process, which is mainly caused by corrosion ions eroding the gap between the inclusion and the steel matrix. The inclusion of steel without rare earth elements is often irregular in shape and large in size, so the corrosion sites are more than those of rare earth steel. The inclusion continues to dissolve in (b) and (e), a small amount of corrosion products is generated, the area of  $\text{Cl}^-$  contact steel matrix becomes larger, and the corrosion range continues to expand; and in (c) and (f), a long-term corrosion process, where more corrosion products accumulate on the surface of the steel. The corrosion products on the surface of EH36 steel are relatively loose, the content of protective  $\alpha\text{-FeOOH}$  is less, and there are more cracks in the products, which provides a channel for  $\text{Cl}^-$  erosion. However, the corrosion products on the surface of steel doped with rare earth elements are closely packed. Rare earth elements promote the generation of  $\alpha\text{-FeOOH}$ , which hinders contact between the steel matrix and the environment.



**Figure 6.** Schematic diagram of corrosion process. The initial corrosion process of EH36 steel (a) and RE-EH36 steel (d); the spreading corrosion process of EH36 steel (b) and RE-EH36 steel (e); the long-term corrosion process of EH36 steel (c) and RE-EH36 steel (f).

### 3.5. Effect of Temperature and $\text{Cl}^-$ Concentration on Corrosion

#### 3.5.1. Effect of Temperature on Corrosion

In order to explore the influence of temperature on corrosion, EH36 offshore platform steel and 1#La steel were immersed in 3.5 wt% NaCl, and different corrosion temperatures were set as 5 °C, 15 °C, 25 °C, 35 °C, and 45 °C, respectively. Nyquist plot (Figure 7a<sub>0</sub>,a<sub>1</sub>) and Tafel polarization curves (Figure 8a<sub>0</sub>,a<sub>1</sub>) were used to explore the influence of temperature on the corrosion of the EH36 and 1#La steel. As the temperature increased, both of them showed the same trend, whereby the radius of capacitive arc resistance decreased. This means that the easier the charge transfer, the more likely corrosion will occur.  $R_{ct}$  values were obtained from the electrochemical equivalent circuit in Figure 4c. The change in  $R_{ct}$  value with temperature is shown in Figure 9a, where the  $R_{ct}$  value gradually decreases with the increase in temperature. The values of  $I_{corr}$  were obtained by extrapolating Tafel, and the variation in  $I_{corr}$  is shown in Figure 9b. With the increase in temperature, the corrosion current density gradually increased, and the corrosion accelerated. Yan et al. [31] reached the same conclusion when they investigated the effect of temperature on the corrosion behavior of E690 steel in a 3.5 wt% NaCl solution. This was due to the increase in temperature, which accelerated the diffusion of ions, resulting in accelerated anodic dissolution of the steel and a decrease in the corrosion resistance of the steel [32].

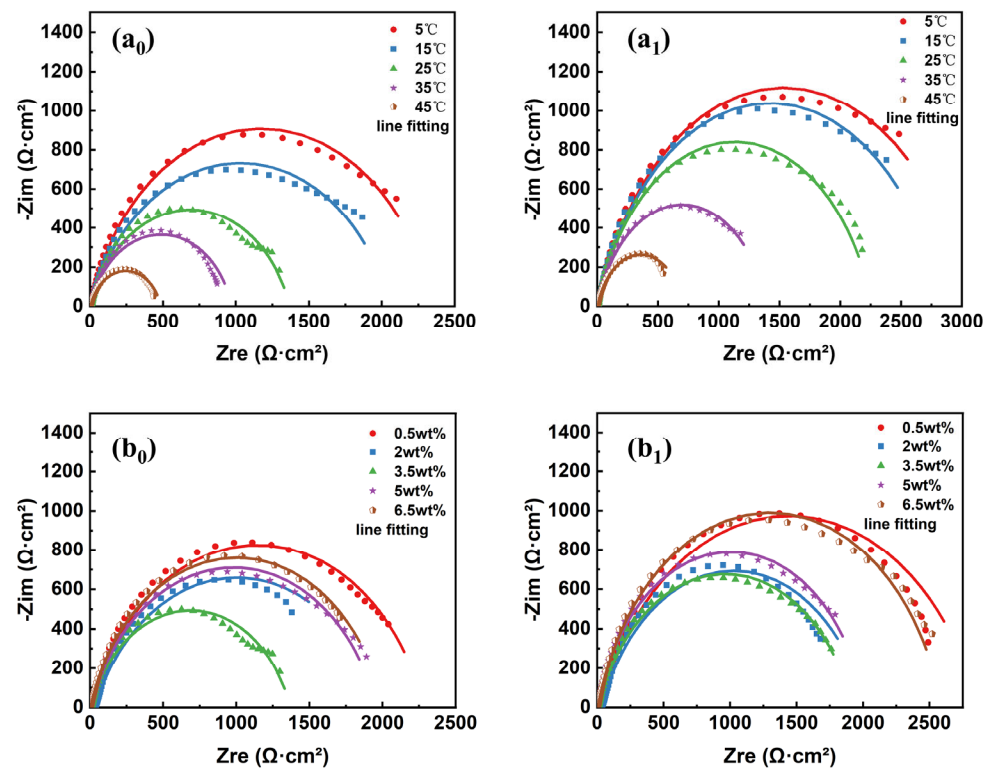


Figure 7. Nyquist plots of the EH36 steel ( $a_0$ ) and La steel ( $a_1$ ) at different temperatures; Nyquist plots of the EH36 steel ( $b_0$ ) and La steel ( $b_1$ ) at different  $Cl^-$  concentrations.

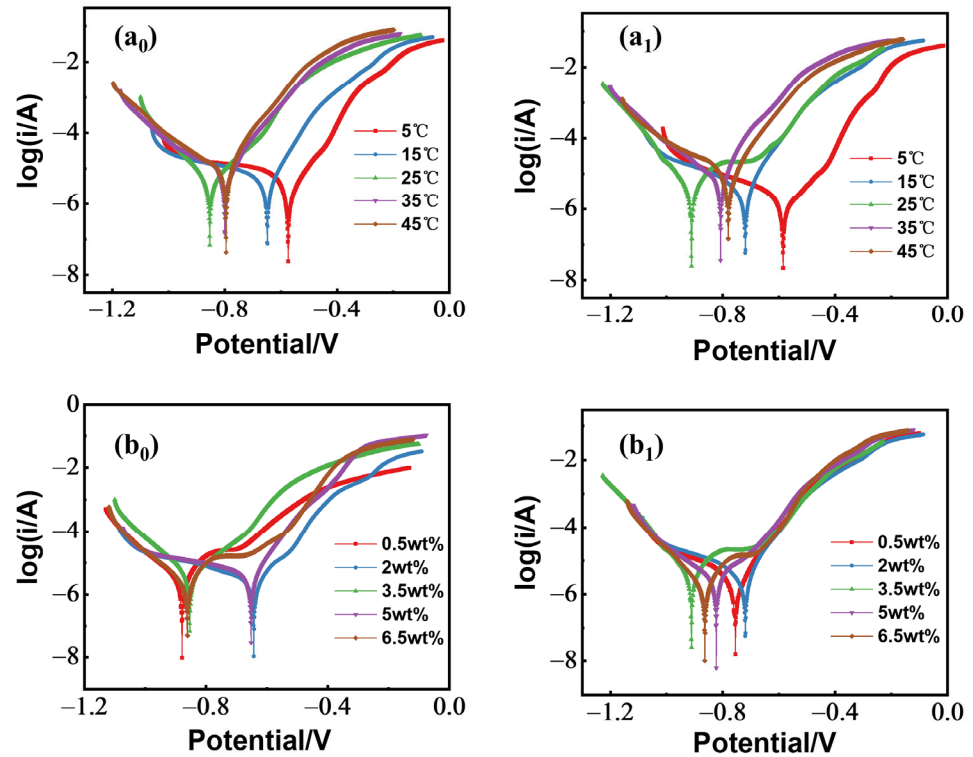
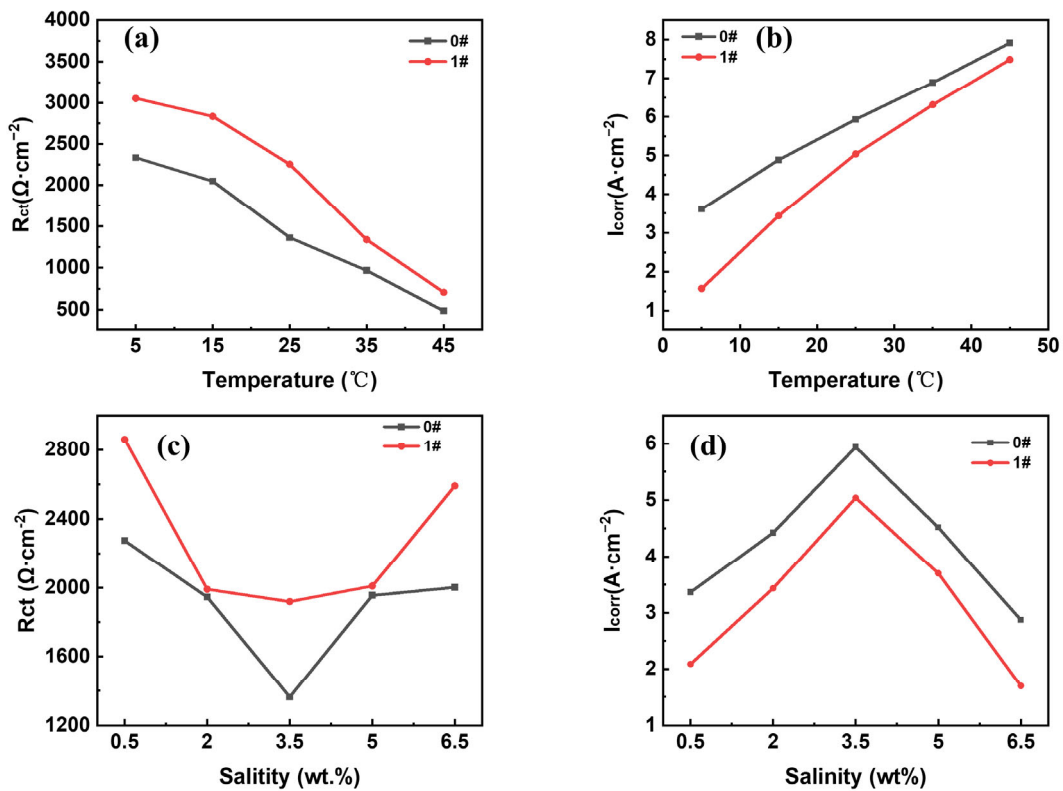


Figure 8. Tafel polarization curves of the EH36 steel ( $a_0$ ) and La steel ( $a_1$ ) at different temperatures; Tafel polarization curves of the EH36 steel ( $b_0$ ) and La steel ( $b_1$ ) at different  $Cl^-$  concentrations.



**Figure 9.**  $R_{ct}$  changes in 0#EH36 steel and 1# La steel at different temperatures (a) and  $\text{Cl}^-$  concentrations (c);  $I_{corr}$  changes in 0#EH36 steel and 1# La steel at different temperatures (b) and  $\text{Cl}^-$  concentrations (d).

### 3.5.2. Effect of $\text{Cl}^-$ Concentration on Corrosion

In order to explore the influence of  $\text{Cl}^-$  concentration on corrosion, EH36 offshore platform steel and 1#La steel were immersed in corrosion solution with a  $\text{Cl}^-$  concentration of 0.5 wt%, 2.0 wt%, 3.5 wt%, 5.0 wt%, and 6.5 wt%, respectively. Nyquist plot (Figure 7b<sub>0</sub>,b<sub>1</sub>) and Tafel polarization curves (Figure 8b<sub>0</sub>,b<sub>1</sub>) were used to explore the influence of  $\text{Cl}^-$  concentration on the corrosion of the two kinds of steel. The variation in the  $R_{ct}$  value with  $\text{Cl}^-$  concentration is shown in Figure 9c; as the  $\text{Cl}^-$  concentration increased, the  $R_{ct}$  value first decreased and then increased.  $I_{corr}$  was obtained by extrapolating Tafel, and the change in  $I_{corr}$  is shown in Figure 9d. The trend of  $I_{corr}$  was just opposite to that of  $R_{ct}$ . Both of the two steels showed the same corrosion trend in different concentrations of  $\text{Cl}^-$  solution; that is, with the increase in  $\text{Cl}^-$  concentration, the corrosion first intensified and then slowed down. The most severe corrosion was observed at a  $\text{Cl}^-$  concentration of 3.5 wt%. Studies [33] have shown that the corrosion solution of 3.0 wt%~3.5 wt% NaCl has the most serious corrosion properties on steel at room temperature. This is mainly because when the salt concentration is lower than 3.5 wt%, the solution conductivity increases with the increase in salinity, so the corrosion rate increases. When the salinity is higher than 3.5 wt%, the dissolved oxygen decreases as the  $\text{Cl}^-$  concentration increases. The concentration of dissolved oxygen is an important factor affecting corrosion [34]. When the  $\text{Cl}^-$  concentration is higher than 3.5 wt%, the corrosion rate is affected by the oxygen concentration together with the conductivity. As the  $\text{Cl}^-$  concentration goes up, the oxygen solubility progressively decreases, which leads to a reduction in the corrosion rate. Conductivity tended to increase with a higher  $\text{Cl}^-$  concentration, which led to an increase in corrosion rate. However, the former corrosion rate reduced to a more significant extent than the latter corrosion rate increased, so the overall corrosion rate shows a downward trend. Li et al. [35], who studied the effect of  $\text{Cl}^-$  concentration on the corrosion of E690 steel, found a similar phenomenon as that described above. Furthermore, the existence of a

film of  $\text{Fe}(\text{OH})_2$  also reduced the dissolved oxygen in the film environment on the metal surface, leading to the weakening of corrosion.

The rare earth elements can improve the corrosion resistance of EH36 steel. The corrosion trend of EH36 steel and La steel at different temperatures and concentrations of  $\text{Cl}^-$  solution is not changed; that is, with the increase in temperature, the corrosion accelerated; with the increase in  $\text{Cl}^-$  concentration, the corrosion first intensified and then slowed down.

#### 4. Conclusions

1. The addition of La, Ce, and Pr can improve corrosion resistance and reduce the corrosion rate of EH36 offshore platform steel. The reason is that more compact corrosion products were formed on the surface of the steel, which promoted the production of more  $\alpha\text{-FeOOH}$  and hindered the further invasion of corrosive ions.
2. The addition of La, Ce, and Pr rare earth elements increased the  $R_{ct}$  and the charge transfer resistance of EH36 offshore platform steel; the Tafel polarization curve moved to the anode and the  $I_{corr}$  decreased, and the corrosion resistance increased.
3. The doped rare earth did not change the effect of temperature and  $\text{Cl}^-$  concentration on corrosion. With the increase in temperature, the corrosion resistance decreased gradually. With the increase in  $\text{Cl}^-$  concentration, the corrosion was first rapid and then slow; the corrosion was the most serious at the salt concentration of 3.5 wt%.

Trace La, Ce, and Pr (less than 0.0004%) can also improve the corrosion resistance of EH36 steel. This provides a further reference for the application of trace rare earth elements.

**Author Contributions:** Conceptualization, L.Q. and X.W.; methodology, S.Z. and X.W.; software, Y.L. and N.L.; validation, A.G., X.W. and L.Q.; data curation, L.Q. and S.Z.; supervision, A.G. All authors have read and agreed to the published version of the manuscript.

**Funding:** This research received no external funding.

**Institutional Review Board Statement:** Not applicable.

**Informed Consent Statement:** Not applicable.

**Data Availability Statement:** Data are contained within the article.

**Conflicts of Interest:** The authors declare no conflicts of interest.

#### References

1. Bhandari, J.; Khan, F.; Abbassi, R.; Garaniya, V. Modelling of pitting corrosion in marine and offshore steel structures—A technical review. *J. Loss Prev. Process Ind.* **2015**, *37*, 39–62. [[CrossRef](#)]
2. Gong, K.; Wu, M.; Xie, F.; Liu, G.X.; Sun, D.X. Effect of  $\text{Cl}^-$  and rust layer on stress corrosion cracking behavior of X100 steel base metal and heat-affected zone in marine alternating wet/dry environment. *Mater. Chem. Phys.* **2021**, *270*, 124826. [[CrossRef](#)]
3. Zhang, N.Y.; Zeng, D.Z.; Xiao, G.Q.; Shang, J.F.; Liu, Y.Z.; Long, D.C.; He, Q.Y.; Singh, A. Effect of  $\text{Cl}^-$  accumulation on corrosion behavior of steels in  $\text{H}_2\text{S}/\text{CO}_2$  methyl-diethanolamine (MDEA) gas sweetening aqueous solution. *J. Nat. Gas Sci. Eng.* **2016**, *30*, 444–454. [[CrossRef](#)]
4. Zhou, Y.L.; Jun, C.; Yang, X.; Liu, Z.Y. Effects of Cr, Ni and Cu on the Corrosion Behavior of Low Carbon Microalloying Steel in a  $\text{Cl}^-$  Containing Environment. *J. Mater. Sci. Technol.* **2013**, *29*, 168–174. [[CrossRef](#)]
5. Liu, B.; Lin, L. Improvement of Corrosion Resistance of Cu-Based Bulk Metallic Glasses by the Microalloying of Mo. *Intermetallics* **2007**, *15*, 679–682. [[CrossRef](#)]
6. Morozov, Y.; Calado, L.M.; Shakoor, R.A.; Raj, R.; Kahraman, R.; Taryba, M.G.; Montemor, M.F. Epoxy coatings modified with a new cerium phosphate inhibitor for smart corrosion protection of steel. *Corros. Sci.* **2019**, *159*, 108128. [[CrossRef](#)]
7. Xu, D.; Lou, C.; Huang, J.; Lu, X.; Xin, Z.; Zhou, C.L. Effect of Inhibitor-Loaded Halloysite Nanotubes on Active Corrosion Protection of Polybenzoxazine Coatings on Mild Steel. *Prog. Org. Coat.* **2019**, *134*, 126–133. [[CrossRef](#)]
8. Li, L.F. Study on the Effect of Vanadium on Hydrogen Corrosion Resistance and Mechanical Properties of X80 Grade Pipeline Steel. Ph.D Thesis, University of Science and Technology Beijing, Beijing, China, 2020.
9. Su, B.X.; Wang, B.B.; Luo, L.S.; Wang, L.; Su, Y.Q.; Xu, Y.J.; Wang, F.X.; Han, B.S.; Huang, H.G.; Guo, J.J.; et al. Effect of Zirconium Content on the Microstructure and Corrosion Behavior of as-Cast Ti-Al-Nb-Zr-Mo Alloy. *J. Mater. Res. Technol.* **2021**, *15*, 4896–4913. [[CrossRef](#)]

10. Post, C.B.; Schoffstall, D.G.; Beaver, H.O. Hot-workability of stainless steel improved by adding cerium and lanthanum. *J. Met.* **1951**, *3*, 973–977. [[CrossRef](#)]
11. Lian, X.T.; Chen, L.; Fan, Z.W.; Liu, T.S.; Xu, D.X.; Dong, H. Effects of Modified Inclusions and Precipitates Alloyed by Rare Earth Element on Corrosion and Impact Properties in Low Alloy Steel. *Acta Metall. Sin. (Engl. Lett.)* **2022**, *35*, 1719–1730. [[CrossRef](#)]
12. Li, H.; Yu, Y.C.; Ren, X.; Zhang, X.H.; Wang, S.B. Evolution of Al<sub>2</sub>O<sub>3</sub>: Inclusions by cerium treatment in low carbon high manganese steel. *J. Iron Steel Res. Int.* **2017**, *9*, 925–934. [[CrossRef](#)]
13. Huang, F.; Li, J.; Geng, R.; Wang, C.C. Effect of rare earth on inclusion evolution and corrosion resistance of HRB400E steel. *Mater. Corros.-Werkst. Korros.* **2023**, *74*, 53–67. [[CrossRef](#)]
14. Liu, T.; Li, N.N.; Liu, C.; Li, J.S.; Zhang, T.Y.; Cheng, X.Q.; Yang, S.F. Attempt to Optimize the Corrosion Resistance of HRB400 Steel Rebar with Cr and RE. *Materials* **2022**, *15*, 8269. [[CrossRef](#)]
15. Dong, R.F.; Li, H.; Zhang, X.Y.; Deng, X.T.; Cui, Q.L.; Chen, J.Q.; Yang, X.; Liang, J.W. The Influence of Rare Earth Elements Lanthanum on Corrosion Resistance of Steel Plate for Offshore Platform. *Mater. Res. Express* **2021**, *8*, 096526.
16. Hou, Y.H.; Zhou, S.L.; Li, G.Q.; Moelans, N. Study on the Occurrence State of Lanthanum in Rust Layer and Mechanism of Its Influence on Invasion State of Corrosion Atoms. *Steel Res. Int.* **2022**, *93*, 2200166. [[CrossRef](#)]
17. Zhang, J.; Su, C.M.; Chen, X.P.; Liu, H.Z.; Zhang, L.F. First-Principles Study on Pitting Corrosion of Al Deoxidation Stainless Steel with Rare Earth Element (La) Treatment. *Mater. Today Commun.* **2021**, *27*, 102204. [[CrossRef](#)]
18. Dong, F.; Yan, R.J.; Yang, Z.J.; Yu, Z.C.; Tian, S.Y. Effect of Cerium on corrosion resistance of 22MnCrNiMo steel. *China Metall.* **2019**, *29*, 30–37.
19. Lian, X.T.; Zhu, J.A.; Wang, R.Q.; Liu, T.S.; Xu, J.; Xu, D.X.; Dong, H. Effects of Rare Earth (Ce and La) on Steel Corrosion Behaviors under Wet-Dry Cycle Immersion Conditions. *Metals* **2020**, *10*, 1174. [[CrossRef](#)]
20. Bao, D.H.; Huang, Y.; Cheng, G.G.; Qiao, T.; Dai, W.X. Effect of Ce content on precipitation behavior of rare earth inclusions in H13 steel. *J. Iron Steel Res. Int.* **2021**, *33*, 792–800.
21. Xi, X.J.; Yang, S.F.; Li, J.S.; Zhao, M.J.; Ye, M.L. Inclusion modification and corrosion resistance optimization of 304 stainless steel containing cerium. *Iron Steel* **2020**, *55*, 20–26.
22. Torkkeli, J.; Saukkonen, T.; Hanninen, H. Effect of MnS inclusion dissolution on carbon steel stress corrosion cracking in fuel-grade ethanol. *Corros. Sci.* **2015**, *96*, 14–22. [[CrossRef](#)]
23. Shimahashi, N.; Muto, I.; Sugawara, Y.; Hara, N. Effects of Corrosion and Cracking of Sulfide Inclusions on Pit Initiation in Stainless Steel. *J. Electrochem. Soc.* **2014**, *161*, 494–500. [[CrossRef](#)]
24. Zhang, S.; Liu, J.; Tang, M.; Zhang, X.; Wu, K.M. Role of rare earth elements on the improvement of corrosion resistance of micro-alloyed steels in 3.5 wt.% NaCl solution. *J. Mater. Res. Technol.* **2021**, *11*, 519–534. [[CrossRef](#)]
25. Zhang, X.; Wei, W.Z.; Lin, C.; Liu, J.; Wu, K.M.; Liu, M. Effects of Niobium and Rare Earth Elements on Microstructure and Initial Marine Corrosion Behavior of Low-Alloy Steels. *Appl. Surf. Sci.* **2019**, *475*, 83–93. [[CrossRef](#)]
26. Zhou, G.; Zhang, H.; Jia, H. Austenite grain growth behavior of X100 pipeline steel. *Heat Treat Met.* **2015**, *40*, 71–75.
27. Yamashita, M.; Miyuki, H.; Matsuda, Y.; Nagano, H.; Misawa, T. The long term growth of the protective rust layer formed on weathering steel by atmospheric corrosion during a quarter of a century. *Corros. Sci.* **1994**, *36*, 283–299. [[CrossRef](#)]
28. Morcillo, M.; Diaz, I.; Cano, H.; Chico, B.; de la Fuente, D. Atmospheric corrosion of weathering steels Overview for engineers. Part I: Basic concepts. *Constr. Build. Mater.* **2019**, *213*, 723–737. [[CrossRef](#)]
29. Wang, Z.F.; Liu, J.R.; Wu, L.X.; Han, R.D.; Sun, Y.Q. Study of the Corrosion Behavior of Weathering Steels in Atmospheric Environments. *Corros. Sci.* **2013**, *67*, 1–10. [[CrossRef](#)]
30. Kamimura, T.; Hara, S.; Miyuki, H.; Yamashita, M.; Uchida, H. Composition and protective ability of rust layer formed on weathering steel exposed to various environments. *Corros. Sci.* **2006**, *48*, 2799. [[CrossRef](#)]
31. Yan, Q.; Yin, Q.; Cui, J.; Wang, X.Y.; Qiao, Y.X.; Zhou, H.L. Effect of temperature on corrosion behavior of E690 steel in 3.5 wt.% NaCl solution. *Mater. Res. Express* **2021**, *8*, 016512–016528. [[CrossRef](#)]
32. Li, Q.S.; Luo, S.Z.; Xing, X.T.; Yuan, J.; Liu, X.; Wang, J.H.; Hu, W.B. Effect of Deep Sea Pressures on the Corrosion Behavior of X65 Steel in the Artificial Seawater. *Acta Metall. Sin. (Engl. Lett.)* **2019**, *32*, 9. [[CrossRef](#)]
33. Becker, W.T.; Shipley, R.J. Volume. 13C Corrosion: Environments and Industries. In *ASM Handbook*; Cramer, S.D., Covino, B., Eds.; ASM International: Almere, The Netherlands, 2006; p. 2379.
34. Yang, X.; Xu, G.M.; Che, C.; Zhu, Z.L.; Chen, X.Z.; Qian, L.F.; Qian, L.; Zhang, N.Q. The effect of dissolved oxygen on the oxidation of an austenitic steel in supercritical water. *Mater. High Temp.* **2022**, *39*, 97–105. [[CrossRef](#)]
35. Li, Z.L.; Song, J.L.; Chen, J.H. Corrosion behavior of a high-strength steel E690 in aqueous electrolytes with different chloride concentrations. *J. Mater. Res. Technol.* **2023**, *22*, 596–604. [[CrossRef](#)]

**Disclaimer/Publisher's Note:** The statements, opinions and data contained in all publications are solely those of the individual author(s) and contributor(s) and not of MDPI and/or the editor(s). MDPI and/or the editor(s) disclaim responsibility for any injury to people or property resulting from any ideas, methods, instructions or products referred to in the content.